Development and numerical validataion of a summertime Land Surface Process and Radiobrightness model

Jasmeet Judge

Center for Remote Sensing, Agricultural and Biological Engineering Department, The University of Florida, P.O.Box 110570, Gainesville, FL, 32611, USA

Linda M. Abriola

Department of Civil and Environmental Engineering, The University of Michigan, 1315 GG Brown, 1301, Beal Ave., Ann Arbor, MI 48109, USA

Anthony W. England

Department of Electrical Engineering and Department of Atmospheric, Oceanic, and Space Sciences, The University of Michigan, 3120, EECS Bldg., 1301, Beal Ave., Ann Arbor, MI 48109, USA

Abstract

The University of Michigan's Land Surface Process and Radiobrightness (LSP/R) model was developed as a step toward linking a traditional SVAT model to satellite microwave observations. The LSP/R model simulates land-air interactions and estimates surface fluxes, temperature and moisture profiles in soil and vegetation, and terrain brightness temperatures when forced with observed weather and sky radiance. In this paper, we present four major modifications to an earlier version of the model and describe three test-scenarios to evaluate accuracy of the numerical methods used in the model. The scenarios included comparing the numerical solution with an analytic solution, evaluating coupled energy and moisture transport for a simple case, and calculating errors in energy and mass balance in the model for a realistic case using field observations. Results from these tests demonstrate the physical self-consistency of the model and its successful implementation for the simple scenarios, and argue for its extendibility to more realistically complex cases.

1 Introduction

Soil Vegetation Atmosphere Transfer (SVAT) models are used to simulate energy, moisture, and momentum fluxes at the lower boundary of Atmospheric General Circulation Models (AGCMs). Examples of SVAT models include Biosphere Atmosphere Transfer Scheme (BATS) (Dickinson et al., 1986, 1993), Simple Biosphere-2 (SiB-2) model (Sellers et al., 1986), Simple SiB (SSiB) (Xue et al., 1991), Land Surface Model (LSM) (Bonan, 1996), and Variable Infiltration Capacity (VIC) model (Liang et al., 1994, 1996). A functional requirement of these models is that they maintain estimates of the stored water field, i.e., estimates of the spatial distribution of water stored in soil, snow, and vegetation that is available to the atmosphere through evaporation and transpiration.

Prognostic AGCMs are initialized with atmospheric temperature and moisture profiles and with sea surface temperatures, all derived largely from satellite observations. Stored water, however, is initialized with climatic soil moisture due to lack of an operational method for estimating the stored water field from satellites. It is well known that the AGCMs' predictions for continental weather and near-term climate are highly sensitive to errors in these stored water estimates (Beljaars et al., 1996).

Microwave brightness, for example at 1.4 GHz, is usefully sensitive to near-surface soil moisture even through vegetation column density exceeding 5 kg/m^2 - about that of mature corn (Jackson et al., 1984; Jackson and O'Neill, 1987; Schmugge and Jackson, 1992). This sensitivity to near-surface moisture enables a satellite technique for realiably inferring the stored water field. While the microwave brightness is sensitive to moisture only in the upper few centimeters of soil, assimilation of near-daily observations using an appropriate SVAT model can yield soil moisture profiles to depths of a meter or more (Entekhabi et al., 1994; Houser et al., 1998; Galantowicz et al., 1999; Lakshmi, 2000; Reichle et al., 2001; Reichle and McLaughlin, 2001; Walker and Houser, 2001; Burke et al., 2001). In effect, the assimilation technique uses the difference between observed and predicted brightness temperatures to correct modeled near-surface soil moisture and these frequently corrected moisture estimates propagate deeper into the soil with time. For assimilation to result in convergence to an accurate moisture profile, there cannot be systematic errors in the SVAT thermal or moisture transport processes, or in the radiobrightness relationship to near-surface soil moisture.

Even though the computational demands of AGCMs have required extensive simplifying parameterizations of SVAT models (Trenberth, 1995), current knowledge of the underlying physics permits highly accurate model simulations of thermal and moisture transport processes in unsaturated soils (Milly, 1982; Cahill and Parlange, 1998). Similarly, the relationship between radiobrightness and profiles of moisture and temperature in soil and vegetation is also fairly well understood (Jackson and Schmugge, 1978; Ulaby et al., 1981; Schmugge and O'Neill, 1986; Njoku and Entekhabi, 1996). The University of Michigan's Microwave Geophysics Group (MGG) has developed a series of terrain-specific physically-based SVAT models that are linked to microwave emission models (Liou and England,

1998a,b; Liou et al., 1999; Galantowicz and England, 1997; Kim, 1999). Unlike most SVAT models intended for use with atmospheric models, the Michigan's Land Surface Process (LSP) models are diagnostic models in that they strive for physical fidelity at the cost of computational complexity. They simulate one-dimensional coupled heat and moisture transport in unsaturated soils (de Vries, 1958; Philip and de Vries, 1957) when forced with observed downwelling short and long-wave radiation, and micro-meteorological observations of air temperature, relative humidity, wind speed, and precipitation. They are initialized with observed soil temperature and moisture profiles augmented at depths below 1 meter with model-based climatic profiles. Estimates of soil and canopy moisture and temperatures from the LSP models are used by the microwave emission or a radiobrightness (R) models to predict brightness temperatures (see Figure 1). As our models evolved, we sought more rigorous means for testing their integrity. In this paper, we present improvements to the LSP/R model for prairie grassland developed by Liou and England (Liou et al., 1999). We also present a rigorous validation of its internal consistency and its agreement with an analytical solution for a simplified system.

2 The Original LSP Model for Prairie Grasslands

2.1 Biophysics and Governing Equations

The LSP model (called 1-dH module in the original model) consists of bi-layered vegetation over a soil whose constitutive properties are constant throughout the profile. Figure 2 shows the land surface processes simulated in the model. Vegetation cover can be assigned from 0% (bare soil) to 100% (continuous canopy). The vegetation includes a photosynthetically active canopy layer and a thermally insulating, non-photosynthetic thatch layer. The thatch has no moisture holding capacity, does not affect the moisture exchanges between the canopy and the soil, but does influence the exchange of radiant energy between the soil and the photosynthetically active layer.

The soil is divided into 60 computational blocks. Because soil closer to the surface is more influenced by rapid changes in weather and downwelling radiance, thicknesses of the blocks increase exponentially with depth. The upper blocks also serve as a root-zone where moisture for transpiration is drawn from the soil, as shown in Figure 2. The constitutive properties of soil, such as moisture and thermal diffusivities, tortuosity, thermal conductivity, and water retention, are estimated from empirical models that have earned acceptance in the literature (de Vries, 1963; Kimball et al., 1976; Lai et al., 1976; Rossi and Nimmo, 1994; Liou and England, 1998a). The moisture and energy balance equations for the soil are (Philip and de Vries, 1957; de Vries, 1958):

$$\frac{\partial X_m}{\partial t} = -\nabla \cdot \vec{q}_m \qquad \frac{\partial X_h}{\partial t} = -\nabla \cdot \vec{q}_h \tag{1a}$$

$$X_m = \rho_l(\theta_l + \theta_v) \qquad X_h = C_m(T - T_0) + L_0\rho_l\theta_v + \rho_l \int_0^{\theta_l} W d\theta \tag{1b}$$

$$\vec{q}_m = -\rho_l(D_T\nabla T + D_\theta \nabla\theta + K\hat{k}) \qquad \vec{q}_h = -\lambda\nabla T + L_0\vec{q}_v + (c_p q_v + c_l q_l)(T - T_0) \quad (1c)$$

where, all the symbols above are defined in section 8.

The moisture and energy fluxes across the upper boundary, i.e., at the interface between soil and vegetation, are driven by net precipitation and radiation reaching the soil surface as follows:

$$q_m(0,1) = \rho_l(D_c - E_s - E_{tr} - Runoff) \quad (2a)$$
$$q_h(0,1) = R_{ns} - H - L \quad (2b)$$

where,
• $q_m(0,1)$ and $q_h(0,1)$ are the moisture and heat flux densities at the interface between blocks 0 (vegetation) and 1 (soil surface), respectively,
• H and L are the sensible and latent heat fluxes from the soil, respectively (W/m^2),
• D_c is the rate of drainage from the canopy (m/s), D_c = tot. precipitation − interception by the canopy,
• E_s is the rate of evaporation from the soil (m/s),
• E_{tr} is rate of transpiration from the root zone (m/s) and,
• R_{ns} is the net radiation (longwave and shortwave) absorbed by the soil (W/m^2)

The energy and moisture fluxes across the lower boundary, i.e., at the interface between the nth and n+1th computational blocks, are set equal to the fluxes across the interface between n-1th and nth block (see Figure 2). This allows no change in the moisture and heat content of the nth block.

2.2 Numerical Algorithm and Implementation

The non-linear and coupled equations for conservation of moisture and energy in soil (1a) are linearized and solved using an explicit, forward finite difference method (Camillo et al., 1983; Liou et al., 1999). In the model, the dynamic response to non-linearity is lagged in time. Combining the equations (1a) through (1c), we obtain two equations of the form:

$$M\frac{\partial\theta_l}{\partial t} + E\frac{\partial T}{\partial t} = X \qquad N\frac{\partial\theta_l}{\partial t} + F\frac{\partial T}{\partial t} = Y \quad (3)$$

where, $X = -\nabla\cdot\frac{\vec{q}_m}{\rho_l}$, $Y = -\nabla\cdot\vec{q}_h$, and M, N, E, and F are defined in section 8. $\frac{\partial\theta_l}{\partial t}$ and $\frac{\partial T}{\partial t}$ represent the temporal changes in moisture content and temperature, respectively. Solving the above equations simultaneously,

$$\frac{\partial\theta_l}{\partial t} = \frac{FX - EY}{MF - EN} \qquad \frac{\partial T}{\partial t} = \frac{MY - NX}{MF - EN} \quad (4)$$

Figure 3 gives a schematic representation of the difference method as implemented in the model. It uses a block-centered grid where the soil parameter values for each computational block are assumed to be located at the center of that block.

A flow diagram of the computations in the LSP model is given in Figure 4. To begin, the soil and the vegetation properties are initialized and the initial energy and moisture fluxes are calculated. The model is forced with weather, and a two-dimensional Newton Raphson technique is applied in conjunction with a finite difference method to balance energy and moisture fluxes at the soil surface. Figure 5 gives a detailed description of the Newton Raphson technique used in the model. The boundary-flux matching process is repeated until a specified convergence criterion is satisfied. The resulting new fluxes are used to estimate the new surface temperature and moisture. Once the surface temperature and moisture are estimated, the difference method is employed to calculate the new fluxes, temperature, and moisture for each soil block.

3 The Radiobrightness (R) Model

The R model estimates the non-scattering emission from a canopy-cloud layer over a semi-infinite, homogeneous, and smooth-surfaced soil. Figure 6 shows the different brightness components of the R model. The net brightness of the terrain is (Liou et al., 1999):

$$T_b = T_{bs} + T_{bc,d} + T_{bc,u} + T_{bsky} \tag{5}$$

where,
• T_{bs} is the emission from soil at the top of the canopy after being attenuated through the canopy (K),
• $T_{bc,d}$ is the downwelling emission from the canopy reflected by the soil and attenuated through the canopy (K),
• $T_{bc,u}$ is the upwelling emission from the canopy (K) and,
• T_{bsky} is the downwelling sky emission reflected by the soil and attenuated through the canopy (K).

The relative permittivity and reflectivity of the soil are estimated from a four-component mixture model by Dobson et al. (1985) and Fresnel equations, respectively. The relative permittivity of the canopy is estimated from the dual-dispersion model by Ulaby and El-Rayes (1987). The attenuation through the canopy depends on its optical depth (τ), which is modeled empirically as (Liou et al., 1999):

$$\tau = \frac{n_c.k.B_c.\mathrm{Exp}\left[\frac{h_c}{0.1149} - 1\right]}{\rho_w} \tag{6}$$

where,
- n_c is the refractive index of the canopy,
- k is the wave number,
- ρ_w is the density of water (kg/m^3),
- B_c is the canopy wet biomass (kg/m^2) and,
- h_c is the canopy canopy height (m).

4 Model Modifications

The LSP model summarized above required modifications to make some parameterizations more bio-physically realistic. For instance, the model had homogeneous soil with uniform constitutive properties. The model had been calibrated only during drydown periods and did not include an infiltration model during precipitation events. The lower boundary condition did not allow for changes in heat and moisture content with time in the lowermost, nth, soil block, as mentioned in section 2.1. The model was also not extendible to different soils because two of the parameters, pore size index and air entry pressure, used in calculating the soil water retention curve were chosen as constants, applicable only to one soil type.

To address these limitations, four modifications were made to the LSP model. The first was to include layers of distinct physical, thermal and hydraulic properties in the soil. Each soil block in the model has uniform constitutive properties throughout its thickness, while the properties vary between the blocks.

The second modification was to generalize the air entry pressure (Ψ_0) and the pore size index (λ_p) parameters employed in a two-parameter junction model developed by Rossi and Nimmo (Rossi and Nimmo, 1994) for estimating soil water retention. In the modified version, these parameters are empirical formulations as functions of soil texture following Rawls et al. (Rawls et al., 1991):

$$\begin{aligned}\lambda_p = &\exp[-0.784 + 0.018S - 1.062\theta_a - 5\text{x}10^{-5}S^2 - 3\text{x}10^{-3}C^2 + \\ &1.111{\theta_a}^2 - 0.031S\theta_a + 3\text{x}10^{-4}S^2{\theta_a}^2 - 6\text{x}10^{-3}C^2{\theta_a}^2 - \\ &2\text{x}10^{-6}S^2C + 8\text{x}10^{-3}C^2\theta_a - 7\text{x}10^{-3}{\theta_a}^2C] \qquad (7)\\ \Psi_0 = &0.01\exp[5.34 + 0.185C - 2.484\theta - .002C^2 - 0.044S\theta_a - \\ &0.167C\theta_a + 1\text{x}10^{-3}S^2{\theta_a}^2 - 0.009C^2{\theta_a}^2 - 1\text{x}10^{-5}S^2C + \\ &9\text{x}10^{-3}C^2\theta_a - 7\text{x}10^{-4}S^2\theta_a + 1\text{x}10^{-6}SC^2 + 0.5{\theta_a}^2C] \qquad (8)\end{aligned}$$

where, S, C and θ_a are the volumes of sand, clay and air in the soil, given in %. Though this formulation has been well tested only for sandy soils, we chose it because it is the best available relationship for deriving the parameters from observed soil properties.

The third modification was to include an infiltration model that accounts for changes

in infiltration with time and with soil properties The maximum infiltration rate (I_{max}), defined as the volume of water per unit area of soil that is allowed into the soil per second (m/sec), depends on soil hydraulic and physical properties, soil temperature, vegetation cover, and surface characteristics like slope and roughness (Ghildyal and Tripathi, 1987). In the modified model, this I_{max} is estimated using a quasi-analytic solution to Richard's equation for vertical infiltration in a homogeneous soil with a constant initial moisture profile (Philip, 1987a, 1957, 1987b; Green and Ampt, 1911). Such a solution (equation 9) can be used because it is applied only to estimate I_{max} at the surface and the soil properties of the surface-block are homogeneous. The transport of moisture in the deeper nodes is governed by the conservation equations given in (1b).

$$i(t) = A + \frac{B}{2} t^{-\frac{1}{2}} \tag{9}$$

where,

$$A = \delta K_{sat}$$
$$B = 2 K_{sat} \Psi_f (\theta_s - \theta_0)$$

where, δ is an empirical parameter set to 0.66 (Philip, 1987a), K_{sat} is the saturated hydraulic conductivity, θ_s is the saturated moisture content, θ_0 is the moisture content before precipitation, and Ψ_f is the matric head of the wetting front estimated as the air entry pressure Ψ_0 (Reible et al., 1990).

The infiltration model included in the LSP model is physically simplistic in that it does not include the affect of ponded water on infiltration rate (I) when precipitation rate (P) is high. When P is less than the estimated I, the model uses P for moisture flux estimation at the surface, otherwise it uses I. Any excess rain during high P is treated as runoff.

The fourth modification was to alter the lower boundary conditions, from conditions on energy and moisture fluxes to conditions on temperature and moisture content. Because the fluxes into and out of the *nth* soil block in the previous model were assumed equal, the heat and the moisture content did not change in the block over time. In the modified model, we set the temperature (T) and moisture (θ) at the *nth* block to be the same as those of the block above ($n-1$), i.e,

$$\theta_m(n) = \theta_m(n-1) \qquad T(n) = T(n-1) \tag{10}$$

This moisture condition implies that there is no capillary-driven force at the lower boundary. It is realistic because the lowermost soil block is at a depth of $\sim$5 m, which corresponds to saturated zones in the Great Plains region. The boundary condition for the temperature implies that there is no heat conduction at boundary. The zero temperature gradient condition is appropriate if the time required for a temperature change at the upper boundary to reach the lower boundary exceeds the duration of the simulation. A temperature change at the surface reaches the lower boundary at 5 m in approximately 73 days, based upon an analytical analysis similar to the one described in Section 5.1. To

explore the behaviour at 5m, a temperature rise of 20 K was introduced at the surface of a 5 m soil column whose initial temperature and volumetric moisture were 293.15 K and 20%, respectively. The moisture was held at the equilibrium value and the lower boundary was closed to moisture or heat flow. Figure 7 shows the temperature profile in the soil after 20, 50, 60, 73, and 80 days. There was a .001 K rise in temperature at the depth of 5 m after day 73. Applications of the model presented here are restricted to 20-30 days. If the simulations were inter-seasonal or annual, then we would need more sophisticated boundary conditions for the lower boundary.

In the R-model, the formulation for canopy optical thickness (τ) was generalized. In the community model, the optical thickness was modeled empirically (6), where the functional dependence of biomass upon canopy height was obtained from a field experiment (Dahl et al., 1993). A modification was necessary to extend the model for different canopy biomass distributions. The modified formulation for τ follows (England and Galantowicz, 1995) and (Ulaby et al., 1983), and is given by:

$$\tau = -\frac{2kn_cB_c}{\rho_c} \tag{11}$$

where,
- ρ_c is the density of wet vegetated material (kg/m^3),
- n_c is the complex refractive index of the canopy,
- B is the wet biomass of the canopy(kg/m^2), and
- k is the wave number. The detailed derivation of τ is given in section 8.

5 Numerical Validation

Because the LSP model is more complex than the R-model, only the former was extensively tested. This section describes three tests conducted to ensure that the numerical simulation in the LSP model is implemented correctly, both qualitatively and quantitatively. This validation was critical because such tests were never conducted during the development of the model. In the first test, the numerical solution is compared with an analytic solution for a simplified transport problem. In the second test, we confirm that the physics of coupled moisture and energy flow is correctly simulated for a homogeneous soil when a symmetric initial temperature profile is used. In the third, we check errors in mass and energy balance for a realistic simulation using inputs from field observations. All the three tests are conducted for bare soil cases (vegetation cover = 0) because the vegetation layer is treated as a separate layer in the model from a numerical standpoint.

5.1 The LSP Numerical Solution vs. an Analytic Solution for a Simple Transport Problem

We verify the quantitative accuracy of the model by comparing the finite difference solution with an analytic solution for a simplified problem chosen to model strong coupling between moisture and heat transport in a dry, vapor-dominated system (Milly, 1982). In this problem, the soil is at an equilibrium temperature (T) and vapor density, (ρ_v) with no heat or moisture flow at the lower boundary. The vapor density is suddenly increased at the upper boundary by ρ_{v0} , while the temperature at the boundary is held constant at T. The vapor diffuses into the soil and releases heat as it condenses. This increases the soil temperatures temporarily, with both the vapor density and the temperatures returning to equilibrium, at their values at the upper boundary (Milly, 1982).

We use an analytic solution for this problem as outlined by Crank (1975) and is described in detail in section 8. To compare the two solutions, we choose Yolo light clay because it has been extensively studied and its properties (see Table 2) are well documented (Philip, 1957; Haverkamp et al., 1977; Milly, 1982). The soil column is 0.1 m thick with the water retention curve given by equations (12a) and (12b). The initial and boundary conditions are given in equations (13a) through (13f). Because the analytic solution is based upon constant soil properties, thermal capacity, latent heat of vaporization, humidity, and thermal conductivity are kept constant in the numerical simulation to achieve a better comparison. The changes in moisture and vapor density with matric potential are also held constant.

$$\theta_m = 0.371\left[1 + \left(\frac{log(\Psi)}{2.26}\right)^4\right]^{-1} + 0.124 \qquad \Psi < 0.01m \tag{12a}$$

$$\theta_m = 0.495 \qquad \Psi \geq 0.01m \tag{12b}$$

$$\rho_v = \rho_v^* \qquad t = 0 \qquad 0 \leqslant z \leqslant 0.1 \tag{13a}$$

$$T = T^* \qquad t = 0 \qquad 0 \leqslant z \leqslant 0.1 \tag{13b}$$

$$\rho_v = \rho_v^* + \rho_{v0} \qquad t \geq 0 \qquad z = 0 \tag{13c}$$

$$T = T^* \qquad t > 0 \qquad z = 0 \tag{13d}$$

$$q_m = 0 \qquad t \geq 0 \qquad z = 0.1m \tag{13e}$$

$$q_h = 0 \qquad t \geq 0 \qquad z = 0.1m \tag{13f}$$

where,
- $T^* = 293.15K$ and,
- $\rho_v^* = 4.03\text{x}10^{-3} kg/m^3$,
- $\rho_{v0} = 0.63\text{x}10^{-3} kg/m^3$.

Figures 11(a) and 11(b) compare the numerical and the analytic solutions for moisture and temperature profiles as time progresses from 10 minutes to 4 days. The temperature

rose as the increased vapor density penetrated into the lower layers and condensed. The system reached equilibrium after ~5 days. The numerical solution follows the analytic solution with a maximum difference of 2.2 mK for temperature and 0.0006 % for moisture over the comparison period.

5.2 Moisture and Energy Flow in a Homogeneous Soil

To confirm the proper implementation of coupled moisture and energy propagation in homogeneous soil profile, the LSP model is run with a symmetric initial temperature profile [Figure 10(a)], a constant initial moisture profile (0.3 m^3/m^3), and zero heat and moisture fluxes at the upper and lower boundaries. The soil is modeled to a depth of 1 m and discretized into 20 blocks of equal thickness and uniform constitutive properties (see Table 1).

Figures 10(a) and 10(b) show the temperature and moisture profiles for selected times during a 43-day model simulation. Heat flows down the temperature gradient, as expected, and the soil achieves equilibrium temperature after ~ 6 days [Figure 10(a)]. The moisture not only follows the negative of the temperature gradient, but it also follows gravity. Because the capillary retention curve is linear in the vicinity of the moisture value of 0.3 m^3/m^3 [Figure 10(c)], the moisture profile at equilibrium is linear with depth [see Figure 10(b)].

5.3 Mass and Energy Balance

The LSP model is tested for the conservation of mass (moisture) and energy. After all the mass and energy fluxes at the boundary, and changes in the fluxes at all the nodes in the soil have been calculated, the following mass and energy balance should hold for the soil as a whole. For each time increment,∂t,

$$q_m(0,1) - q_m(n,n+1) = \sum_{i=1}^{n} \partial(X_m)_i \Delta z_i \tag{14a}$$

$$q_h(0,1) - q_h(n,n+1) = \sum_{i=1}^{n} \partial(X_h)_i \Delta z_i \tag{14b}$$

where, Δz_i is thickness of the ith soil-block, $q_m(0,1)$, $q_h(0,1)$, $q_m(n,n+1)$, $q_h(n,n+1)$, $\partial(X_m)$, and $\partial(X_h)$ are defined in previous sections.

Differences between the left and the right hand sides of equations (14a) and (14b) represent the instantaneous errors in moisture balance (err_{mb}), and in energy balance (err_{eb}),

respectively. The cumulative relative errors (CREs) for mass, err_{rm}, and for energy, err_{re}, are calculated with respect to the maximum of moisture and energy fluxes at the upper and the lower boundaries as shown in equations (15a) and (15b), respectively. After a time interval, t_f,

$$err_{rm} = \frac{\sum_{t=1}^{t_f} (err_{mb})_t}{\sum_{t=1}^{t_f} max\left[|q_m(0,1)|, |q_m(n,n+1)| \right]} \tag{15a}$$

$$err_{re} = \frac{\sum_{t=1}^{t_f} (err_{eb})_t}{\sum_{t=1}^{t_f} max\left[|q_h(0,1)|, |q_h(n,n+1)| \right]} \tag{15b}$$

The CREs are used to evaluate accuracy of the numerical solution. Figures 8 and 9 show these errors for a 12-day bare-soil model simulation during summertime, from Julian day 193 (June 11) through day 205 (June 23) in 1996. Weather forcings to run the model are obtained from our fourth Radiobrightness Energy Balance Experiment (REBEX-4) (Judge and England, 1999). These forcings include incoming radiant fluxes, air temperature, relative humidity, wind, and precipitation. The initial and boundary conditions for the simulation are discussed in detail in Judge (1999). The time-step for the simulation is 3 sec. The soil is modeled up to 5 m, with 9 nodes in the upper 5.5 cm [1]. Soil constitutive properties are constant with depth as given in Table 1.

The CREs are negligible, relative to the magnitude of the incoming heat and moisture fluxes, throughout the simulation period [Figures 8(a) and 9(a)]. Figures 8(b) and 9(b) present magnitude of instantaneous errors in mass and energy balance, respectively. The errors are very small, with the maximum error in moisture balance of $5\text{x}10^{-7}$ kg/m^2 and in energy balance of 2 J/m^2. Figure 8(c) shows the net moisture flux entering the upper boundary, with precipitation on Julian days 194, 196, 198, and 203. Figure 9(c) shows the net incoming energy flux at the upper boundary which is primarily driven by insolation. Throughout the simulation period, energy fluxes vary slowly with time during the night and during clear days (Julian day 197 and 200), but change rapidly during partly cloudy days. Note that maximum errors coincide with the largest surface fluxes.

[1] The conditions on time-step and number of nodes were obtained from convergence tests conducted with the REBEX-4 data and are described in (Judge, 1999).

6 Summary

An LSP/R model, developed for prairie soils, was improved and validated for its accuracy in implementation of the numerical methods. The numerical solution was compared with an analytic solution for strongly coupled moisture and energy transport in a vapor-dominated homogeneous soil. The two solutions compared well, with the maximum differences of 2.2 mK for temperature and 6x10^{-4} % for volumetric soil moisture. The model was tested for heat and moisture transport in a homogeneous soil with constant initial temperature and moisture profiles. The modeled energy propagated down the temperature gradient, and the moisture followed the negative of the temperature gradient and also followed gravity. The equilibrium profile for the soil moisture matched the slope of the soil-water retention curve. The modified LSP model was shown to conserve mass and energy in a more realistic case using inputs from field observations. The maximum errors in mass and energy were 5x10^{-7} kg/m^2 and 2 J/m^2, respectively, for a 12-day simulation period. These tests demonstrate the validity of the modified LSP/R model for the simple test-scenarios, and its extendability to a more complex case.

7 Acknowledgements

Support for this research was provided by grants from the NASA Land Surface Hydrology Program.

8 Appendix

8.1 Simplification of Conservation Equations

The conservation of mass and energy equations are simplified following (de Vries, 1958) prior to applying the finite difference method to solve for temporal changes in soil temperature and moisture profiles.

Conservation of Mass

$$\frac{\partial X_m}{\partial t} = -\nabla \cdot \vec{q}_m \tag{16}$$

$$X_m = \rho_l(\theta_l + \theta_v) \qquad \vec{q}_m = \vec{q}_l + \vec{q}_v \qquad \frac{\partial(\theta_l + \theta_v)}{\partial t} = -\frac{1}{\rho_l}\nabla \cdot \vec{q}_m \tag{17}$$

$$\frac{\vec{q}_l}{\rho_l} = -D_{\theta l} - D_{Tl}\nabla T - K\hat{k} \qquad \frac{\vec{q}_v}{\rho_l} = -D_{\theta v} - D_{Tv}\nabla T \qquad \frac{\vec{q}_m}{\rho_l} = -D_\theta - D_T\nabla T - K\hat{k} \tag{18}$$

$$\frac{\partial \theta_l}{\partial t} = -\nabla \cdot \frac{\vec{q}_l}{\rho_l} - \mathbb{E} \qquad \frac{\partial \theta_v}{\partial t} = -\nabla \cdot \frac{\vec{q}_v}{\rho_l} + \mathbb{E} \tag{19}$$

where,

- X_m is the total moisture content per unit volume (kg/m^3),
- $\vec{q}_l$, $\vec{q}_v$, and $\vec{q}_m$ are the liquid, vapor and moisture flux densities ($kg/m^2.sec$), respectively,
- ρ_l is the density of liquid water (kg/m^3),
- θ_l and θ_v are the volumetric liquid water (m^3/m^3) and vapor content (m^3 of precipitable water/m^3), respectively, and $\theta = \theta_l + \theta_v$,
- T is the absolute temperature (K),
- D_T and D_θ are the thermal and isothermal moisture (liquid and vapor) diffusivities ($m^2/K.s$), respectively,
- K is the unsaturated hydraulic conductivity (m/s), and
- $\mathbb{E}$ is the rate of evaporation (sec^{-1})

From equation (3) in (de Vries, 1958), θ_v can be defined as

$$\theta_v = (P - \theta_l)\frac{\rho_0 h}{\rho_l}$$

- P is the porosity m^3/m^3,
- ρ_0 is the density of saturated water vapor kg/m^3, and
- h is the relative humidity

Taking the derivative of θ_v with respect to time, t,

$$\frac{\partial \theta_v}{\partial t} = -\frac{\rho_v}{\rho_l}\left[\frac{\partial \theta_l}{\partial t}\right] + \frac{P-\theta_l}{\rho_l}\left[h\frac{\partial \rho_0}{\partial t} + \rho_0\frac{\partial h}{\partial t}\right]$$

$\rho_0 = f(T)$ and $h = f(T, \theta_l)$,

$$\frac{\partial \theta_v}{\partial t} = \left[\frac{\rho_0(P-\theta_l)}{\rho_l}\frac{\partial h}{\partial \theta_l} - \frac{\rho_v}{\rho_l}\right]\frac{\partial \theta_l}{\partial t} + \frac{P-\theta_l}{\rho_l}\left[h\frac{\partial \rho_0}{\partial T} + \rho_0\frac{\partial h}{\partial T}\right]\frac{\partial T}{\partial t} \tag{20}$$

Inserting $\frac{\partial \theta_v}{\partial t}$ from equation 20 in 17 and using $\frac{\vec{q}_m}{\rho_l}$ from equation 18,

$$\left\{1 + \frac{\rho_0(P-\theta_l)}{\rho_l}\frac{\partial h}{\partial \theta_l} - \frac{\rho_v}{\rho_l}\right\}\frac{\partial \theta_l}{\partial t} + \frac{P-\theta_l}{\rho_l}\left\{h\frac{\partial \rho_0}{\partial T} + \rho_0\frac{\partial h}{\partial T}\right\}\frac{\partial T}{\partial t} = \nabla \cdot \left[D_\theta \nabla \theta_l + D_T \nabla T + K\hat{k}\right] \tag{21}$$

Conservation of Energy

$$\frac{\partial X_h}{\partial t} = -\nabla \cdot \vec{q}_h \tag{22}$$

From equations (10) and (11) in (de Vries, 1958),

$$\begin{aligned} X_h &= C_d(T-T_0) + L_0\rho_l\theta_v + c_p\rho_l\theta_v(T-T_0) \\ &\quad + c_l\rho_l\theta_l(T-T_0) - \rho_l\int_0^{\theta_l} W\ d\theta_l \qquad (23) \\ \vec{q}_h &= -\lambda\nabla T + L_0\vec{q}_v + c_p(T-T_0)\vec{q}_v + c_l(T-T_0)\vec{q}_l \qquad (24) \end{aligned}$$

where,

- X_h is the total heat content per unit volume (J/m^3),
- $\vec{q}_h$ is the heat flux density $(J/m^2.s)$, respectively,
- C_m and C_d are the volumetric heat capacities of moist and dry soils $(J/m^3.K)$, respectively,
- c_p and c_l are the specific heats $(J/kg.K)$ of water vapor at constant pressure and of liquid water, respectively,
- L_0 is the latent heat of vaporization (J/kg) at the reference temperature, T_0,

- W is the differential heat of wetting, and
- λ is the thermal conductivity of soil $(J/m.K.s)$.

Taking the derivative of 23 with respect to time,

$$\begin{aligned}\frac{\partial X_h}{\partial t} = & C_d \frac{\partial T}{\partial t} + \rho_l \Big[L_0 + c_p (T - T_0) \Big] \frac{\partial \theta_v}{\partial t} \\ & + c_l \rho_l (T - T_0) \frac{\partial \theta_l}{\partial t} - \rho_l W \frac{\partial \theta_l}{\partial t} \end{aligned} \tag{25}$$

Taking the divergence of 24 and substituting $\nabla \cdot \frac{\vec{q}_v}{\rho_l}$ and $\nabla \cdot \frac{\vec{q}_l}{\rho_l}$ from 19,

$$\begin{aligned} -\nabla \cdot \vec{q}_h = & \lambda \nabla \cdot (\nabla T) - c_p \vec{q}_v \cdot \nabla T - c_l \vec{q}_l \cdot \nabla T + L_0 \rho_l \frac{\partial \theta_v}{\partial t} \\ & + c_p \rho_l (T - T_0) \frac{\partial \theta_v}{\partial t} + c_l \rho_l (T - T_0) \frac{\partial \theta_l}{\partial t} - L_0 \rho_l \mathbb{E} \\ & - c_p \rho_l (T - T_0) \mathbb{E} + c_l \rho_l (T - T_0) \mathbb{E} \end{aligned} \tag{26}$$

Equating 25 and 26

$$C_d \frac{\partial T}{\partial t} - \rho_l W \frac{\partial \theta_l}{\partial t} = \lambda \nabla \cdot (\nabla T) - c_p \vec{q}_v \cdot \nabla T - c_l \vec{q}_l \cdot \nabla T - L \rho_l \mathbb{E} \tag{27}$$

Solving for $\mathbb{E}$ from equations 19, 18, and 20,

$$\begin{aligned} \mathbb{E} = & \frac{\partial \theta_v}{\partial t} + \frac{1}{\rho_l} \nabla \cdot \vec{q}_v \\ \mathbb{E} = & \left[\frac{\rho_0 (P - \theta_l)}{\rho_l} \frac{\partial h}{\partial \theta_l} - \frac{\rho_v}{\rho_l} \right] \frac{\partial \theta_l}{\partial t} + \frac{P - \theta_l}{\rho_l} \left[h \frac{\partial \rho_0}{\partial T} + \rho_0 \frac{\partial h}{\partial T} \right] \frac{\partial T}{\partial t} \\ & - \nabla \cdot \Big[D_{\theta_v} \nabla \theta_l + D_{T_v} \nabla T \Big] \end{aligned} \tag{28}$$

Substituting $\mathbb{E}$ from 28, and $\vec{q}_v$ and $\vec{q}_l$ from 18 into 27,

$$\begin{aligned} & \left\{ L \rho_0 (P - \theta_l) \frac{\partial h}{\partial \theta_l} - L \rho_v - \rho_l W \right\} \frac{\partial \theta_l}{\partial t} + \left\{ C_d - L (P - \theta_l) \left[h \frac{\partial \rho_0}{\partial T} + \rho_0 \frac{\partial h}{\partial T} \right] \right\} \frac{\partial T}{\partial t} = \\ & \nabla \cdot \Big[(\lambda - L \rho_l D_{T_v}) \nabla T \Big] + L \rho_l \nabla \cdot (D_{\theta_v} \nabla \theta_l) + \rho_l \Big[(c_p \ D_{\theta_v} + c_l \ D_{\theta_l}) \nabla \theta_l \\ & + (c_p D_{T_v} + c_l D_{T_l}) \nabla T + c_l K \hat{k} \Big] \cdot \nabla T \end{aligned} \tag{29}$$

Defining M and E as the coefficients from 21 and N and F from 29 for equation 3 in section 2.2 as follows:

$$\mathrm{M} = 1 + \frac{\rho_0(P-\theta_l)}{\rho_l}\frac{\partial h}{\partial \theta_l} - \frac{\rho_v}{\rho_l} \tag{30}$$

$$\mathrm{E} = \frac{P-\theta_l}{\rho_l}\left[h\frac{\partial \rho_0}{\partial T} + \rho_0\frac{\partial h}{\partial T}\right] \tag{31}$$

$$\mathrm{N} = L\rho_0(P-\theta_l)\frac{\partial h}{\partial \theta_l} - L\rho_v - \rho_l W \tag{32}$$

$$\mathrm{F} = C_d - L(P-\theta_l)\left[h\frac{\partial \rho_0}{\partial T} + \rho_0\frac{\partial h}{\partial T}\right] \tag{33}$$

8.2 Analytic Solution for Section 5.1

An analytic solution for the problem described in section 5.1 follows Crank (1975). Equations 34a and 34b can be linearized in the form 34c and 34d.

$$D\frac{\partial^2 \rho_v}{\partial z^2} - \frac{\partial}{\partial t}(\rho_v - \lambda_c T) = 0 \tag{34a}$$

$$\mathbb{D}\frac{\partial^2 T}{\partial z^2} - \frac{\partial}{\partial t}(T - \nu_c \rho_v) = 0 \tag{34b}$$

$$\Delta\rho_v = \rho_{v0}F_1 + f(F_1, F_2, \rho_{v0}, T_0) \tag{34c}$$

$$\Delta T = T_0 F_2 + f(F_1, F_2, \rho_{v0}, T_0) \tag{34d}$$

where D, $\mathbb{D}$, λ_c and ν_c are constants that depend on soil properties (Crank, 1975),
• ρ_{v0} and T_0 are the initial changes in vapor density (kg/m^3) and temperature (K) forced at the upper boundary, respectively. ($T_0 = 0$ for the problem in section 5.1) and,
• $\Delta\rho_v$ and ΔT are the changes in vapor density and temperature profiles as functions of time.

The first terms on the right hand sides of the equations 34c and 34d represent the solution if the diffusion of vapor density and temperature were de-coupled. The soil would come to an equilibrium with $\Delta\rho_v = \rho_{v0}$ and $\Delta T = T_0$, as functions F_1 and F_2 increased from $0 \rightarrow 1$ when time increased from $0 \rightarrow \infty$. The second terms represent the solution from coupling between the two diffusion processes.

The forms of F_1 and F_2 depend on the shape of the medium. The soil can be modeled as a plane sheet of thickness, n, and F_1 and F_2 become

$$F_1 = \sum_{i=0}^{\infty}(-1)^i \text{erfc}\frac{(2i+1)z-n}{2\sqrt{Dt}} + \sum_{i=0}^{\infty}(-1)^i \text{erfc}\frac{(2i+1)z+n}{2\sqrt{Dt}} \tag{35a}$$

$$F_2 = \sum_{i=0}^{\infty}(-1)^i \text{erfc}\frac{(2i+1)z-n}{2\sqrt{\mathbb{D}t}} + \sum_{i=0}^{\infty}(-1)^i \text{erfc}\frac{(2i+1)z+n}{2\sqrt{\mathbb{D}t}} \tag{35b}$$

where,
- erfc $x = 1 - \frac{2}{\pi^{1/2}}\int_0^x \exp(-\eta^2)\mathrm{d}\eta$,
- z is the depth in soil (m) and,
- t is the time (sec).

The change in temperature, ΔT, vapor density, $\Delta\rho_v$, and moisture, ΔV_f, as functions of depth and time are given by Crank (1975) as follows:

$$\Delta T = T_0 F_2 - \frac{(1-{\mu_2}^2\mathbb{D})T_0 - \nu_c\rho_{v0}}{\mathbb{D}({\mu_1}^2 - {\mu_2}^2)}(F_2 - F_1) \tag{36a}$$

$$\Delta\rho_v = \rho_{v0}F_1 - \frac{(1-{\mu_1}^2 D)\rho_{v0} - \lambda_c T_0}{D({\mu_1}^2 - {\mu_2}^2)}(F_2 - F_1) \tag{36b}$$

$$\Delta V_f = \sigma_c \Delta\rho_v - \omega_c \Delta T \tag{36c}$$

where,

$${\mu_1}^2 = \frac{1}{D} + \frac{\lambda_c\nu_c}{\mathbb{D}-D} \qquad {\mu_2}^2 = \frac{1}{\mathbb{D}} - \frac{\lambda_c\nu_c}{\mathbb{D}-D}$$

$$\sigma_c = \frac{\partial V_f}{\partial\rho_v} \qquad \omega_c = \frac{\partial V_f}{\partial T}$$

The equation (1a) can be linearized to match the form of equations 34a and 34b if we assume negligible transport of sensible heat by water vapor and negligible liquid flow, as follows (Milly, 1982),

$$\theta_a\frac{\partial\rho_v}{\partial t} + (\rho_l - \rho_v)\frac{\partial\theta_m}{\partial t} = \frac{\partial}{\partial z}\left[D_m\frac{\partial\rho_v}{\partial z}\right] \tag{37a}$$

$$C_m\frac{\partial T}{\partial t} - \rho_l(L+W)\frac{\partial\theta_m}{\partial t} = \frac{\partial}{\partial z}\left[\left(\lambda - D_m\frac{\partial\rho_v}{\partial T}\bigg|_\Psi\right)\frac{\partial T}{\partial z}\right] \tag{37b}$$

where,

$$L = L_0 + (c_p - c_l)(T - T0)$$

- θ_a, ρ_v, ρ_l, λ, C_m, c_l, c_p, L_0, T, T_0 and W have been defined for equation 1b,
- θ_m is the volumetric moisture content (m^3/m^3),
- D_m is an effective molecular diffusivity (m^2/sec) and,
- Ψ is the matric head (m).

References

Beljaars, A., Viterbo, P., Miller, M., Betts, A., 1996. The anomalous rainfall over the us during July 1993 - Sensitivity to land-surface parametrization and soil moisture. *Month. Weat. Rev.* 124 (3), 362–383.

Bonan, G., January 1996. A Land Surface Model (LSM Version 1.0) for ecological, hydrological, and atmospheric studies: Technical description and user's guide. Tech. Rep. NCAR/TN-417+STR, Climate and Global Dynamics Division, NCAR.

Burke, E., Shuttleworth, W., Lee, K., Bastidas, L., 2001. Using area-average remotely sensed surface soil moisture in multipatch land data assimilation systems. *IEEE Trans. Geosci. Remote Sensing* 39 (10), 2091–2100.

Cahill, A., Parlange, M., April 1998. On water vapor transport in field soils. *Water Res. Research* 34 (4), 731–739.

Camillo, P., Gurney, R., Schmugge, T., April 1983. A soil and atmosphere boundary layer model for evapotranspiration and soil moisture studiess. *Water Res. Research* 19 (2), 371–380.

Crank, J., 1975. The Mathematics of Diffusion. Clarendon Press: Oxford.

Dahl, P., Judge, J., Gallo, J., England, A., 1993. Vertical distribution of biomass and moisture in a prairie grass canopy. Tech. Rep. Rad. Lab. Tech. Note RL-902, University of Michigan.

de Vries, D., 1958. Simultaneous transfer of heat and moisture in porous media. *Trans. Am. Geophys. Union* 39 (5), 909–16.

de Vries, D., 1963. Thermal properties of soils. In: Physics of Plant Environment. Interscience Publishers: New York, pp. 210–235.

Dickinson, R., Henderson-Sellers, A., Kennedy, P., August 1993. Biosphere-atmosphere transfer scheme (BATS) version 1e as coupled the NCAR Community Climate Model. Tech. Rep. NCAR/TN-387+STR, Climate and Global Dynamics Division, NCAR.

Dickinson, R., Henderson-Sellers, A., Kennedy, P., Wilson, M., December 1986. Biosphere-atmosphere transfer scheme (BATS) for the NCAR Community Climate Model. Tech. Rep. NCAR/TN-275+STP, Atmospheric Analysis and Prediction Division, NCAR.

Dobson, M., Ulaby, F., Hallikainen, M., El-Rayes, M., 1985. Microwave dielectric behavior of wet soil-part II: Dielectric mixing models. *IEEE Trans. Geosci. Remote Sensing* GE-23, 35–46.

England, A., Galantowicz, J., April 1995. Moisture in a grass canopy from SSM/I radiobrightness. In: Proc. 2nd Tropical Symposium on Combined Optical-Microwave Earth and Atmos. Sensing. Vol. Atlanta, GA. pp. 12–14.

Entekhabi, D., Nakamura, H., Njoku, E., March 1994. Solving the inverse problem for soil moisture and temperature profiles by sequential assimilation of multifrequency remotely sensed observations. *IEEE Trans. Geosci. Remote Sensing* 32 (2).

Galantowicz, J., England, A., September 1997. Seasonal snowpack radiobrightness interpretation using a SVAT-linked emission model. *J. Geophys. Res.* 102 (D18), 21933–46.

Galantowicz, J., Entekhabi, D., Njoku, E., 1999. Tests of sequential data assimilation for retrieving profile soil moisture and temperature from observed l band radiobrightness. *IEEE Trans. Geosci. Remote Sensing* 37 (4), 1860–1870.

Ghildyal, B., Tripathi, R., 1987. Soil physics. John Wiley:New York.

Green, W., Ampt, G., 1911. Studies on soil physics. J. Agri. Sc. 4 (5), 1.

Haverkamp, R., Vauclin, M., Tauma, J., Wierenga, P., Vachaud, G., 1977. A comparison of numerical simulation models for one- dimensional infiltration. *Soil Sci. Soc. Am. J.* 41 (2), 285–294.

Houser, P., Shuttleworth, W., Famiglietti, J., Gupta, H., Syed, K., Goodrich, D., December 1998. Integration of soil moisture remote sensing and hydrologic modeling using data assimilation. *Water Res. Research* 34 (12).

Jackson, T., O'Neill, P., 1987. Temporal observations of surface soil moisture using a passive microwave sensor. *Remote Sens. Env.* 21, 281–296.

Jackson, T., Schmugge, T., 1978. Passive microwave remote sensing of soil moisture. *Advances in Hydroscience* 14, 123–58.

Jackson, T., Schmugge, T., O'Neill, P., 1984. Passive microwave remote sensing of soil moisture from an aircraft platform. *Remote Sens. Env.* 14, 135–142.

Judge, J., 1999. Land surface process and radiobrightness modeling of the great plains. Ph.D. thesis, University of Michigan.This reference will be changed to a paper that has been submitted elsewhere once it is accepted.

Judge, J., England, A., 1999. Field data report for the fourth radiobrightness energy balance experiment (REBEX-4): June - september 1996. Tech. Rep. Rad. Lab. Tech. Note RL-974, University of Michigan.

Kim, E., 1999. Remote sensing of land surface conditions in arctic tundra regions for climatological applications using microwave radiometry. Ph.D. thesis, University of Michigan.

Kimball, B., Jackson, R., Reginato, R., Nakayama, F., Idso, S., 1976. Comparison of field-measured and calculated soil-heat fluxes. *Soil Sci. Soc. Am. J.* 40, 18–25.

Lai, S., Tiedje, J., Erickson, A., 1976. In situ measurement of gas diffusion coefficients in soils. *Soil Sci. Soc. Am. Proc.* 40, 3–6.

Lakshmi, V., 2000. A simple surface temperature assimilation scheme for use in land surface models. *Water Res. Research* 36 (12), 3687–3700.

Liang, X., Lettenmaier, D., Wood, E., Burges, S., July 1994. A simple hydrologically based model of land surface water and energy fluxes for general circulation models. *J. Geophys. Res.* 99 (D7), 14415–14428.

Liang, X., Lettenmaier, D., Wood, E., Burges, S., September 1996. One-dimensional stastical dynamical representation subgrid spatial variability of precipitation in the 2-layer variable infiltration capacity model. *J. Geophys. Res.* 101 (D16), 21403–21422.

Liou, Y., England, A., January 1998a. A land surface process / radiobrightness model with coupled heat and moisture transport in soil. *IEEE Trans. Geosci. Remote Sensing* 36 (1), 273–286.

Liou, Y., England, A., March 1998b. A land surface process/radiobrightness model with coupled heat and moisture transport for freezing soils. *IEEE Trans. Geosci. Remote Sensing* 36 (2), 669–677.

Liou, Y., Galantowicz, J., England, A., 1999. A land surface process/radiobrightness model with coupled heat and moisture transport for prairie grassland. *IEEE Trans. Geosci. Remote Sensing* 37 (4), 1848–1859.

Milly, P., June 1982. Moisture and heat transport in hysteretic, inhomogeneous porus

media: A matric head-based formulation and a numerical method. *Water Res. Research* 18 (3), 489–498.

Njoku, E., Entekhabi, D., 1996. Passive microwave remote sensing of soil moisture. *J. Hydrology* 184, 101–129.

Philip, J., 1957. Theory of infiltration, 1. The infiltration equation and its solution. *Soil Sc.* 83 (5), 345–357.

Philip, J., 1987a. Inverse solution for one-dimensional infiltration and ratio A/K1. *Water Res. Research* 26 (9), 2023–2027.

Philip, J., 1987b. The infiltration joining problem. *Water Res. Research* 23 (12), 2239–2245.

Philip, J., de Vries, D., 1957. Moisture movement in porous materials under temperature gradients. *Trans. Am. Geophys. Union* 38 (2), 222–232.

Rawls, W., Gish, T., Brakensiek, D., 1991. Estimating soil water retention from soil physical properties and characteristics. *Adv. in Soil Sc.* 16, 213–234.

Reible, D., Illangasekare, T., Doshi, D., Malhiet, M., 1990. Infiltration of immiscible contaminants in unsaturated zone. *Ground Water* 28 (5), 685–692.

Reichle, R.H., D. E., McLaughlin, D., September 2001. Downscaling of radiobrightness measurements for soil moisture estimation: A four-dimensional variational data assimilation approach. *Water Res. Research* 37 (9), 2353–2364.

Reichle, R., McLaughlin, D., Entekhabi, D., August 2001. Variational data assimilation of microwave radiobrightness observations for land surface hydrologic applications. *IEEE Trans. Geosci. Remote Sensing* 39 (8), 1708–1718.

Rossi, C., Nimmo, J., March 1994. Modeling of soil water retention from saturation to oven dryness. *Water Res. Research* 30 (3), 701–8.

Schmugge, T., Jackson, T., July 1992. A dielectric model of the vegetation effects on the microwave emission from soils. *IEEE Trans. Geosci. Remote Sensing* 30 (4), 757–760.

Schmugge, T., O'Neill, P., January 1986. Passive microwave soil moisture research. *IEEE Trans. Geosci. Remote Sensing* GE-24 (1), 12–22.

Sellers, P., Mintz, Y., Sud, Y., Dalcher, A., March 1986. A Simple Biosphere model SiB for use within general circulation models. *J. Atmos. Sc.* 43 (6), 505–531.

Trenberth, K. E., 1995. Climate System Modeling. Cambridge University Press: New York.

Ulaby, F., El-Rayes, M., September 1987. Microwave dielectric spectrum of vegetation-PartII: Dual- dispersion model. *IEEE Trans. Geosci. Remote Sensing* GE-25, 550–557.

Ulaby, F., Moore, R., Fung, A., 1981. Microwave Remote Sensing Active and Passive, Vol I. Artech House:Massachussetts.

Ulaby, F., Razani, M., Dobson, M., 1983. Effects of vegetation cover on the microwave radiometeric sensitivity to soil moisture. *IEEE Trans. Geosci. Remote Sensing* GE-21, 51–61.

Walker, J., Houser, P., 2001. A methodology for initializing soil moisture in a global climate model: Sssimilation of near-surface soil moisture observations. *J. Geophys. Res.* 106 (D11), 11761–11774.

Xue, Y., Sellers, P., Kinter, J., Shukla, J., March 1991. A simplified biosphere model for global climate studies. *J. Clim.* 4, 345–364.

FIGURE CAPTIONS

Fig. 1. A flow diagram of interactions between the LSP and R models in the LSP/R model.
Fig. 2. Land surface processes simulated in the LSP model [adapted from (Liou et al., 1999)].
Fig. 3. A schematic representation of the finite difference method used in the LSP model.
Fig. 4. A flow diagram of LSP model algorithm.
Fig. 5. A schematic representation of the computations in the 2-D Newton Raphson Technique in the LSP model.
Fig. 6. Brightness components in the R model.
Fig. 7. Results from an analytic solution to calculate the time necessary for a thermal pulse at the surface to reach the lower boundary at the depth of 5 m. (a) Temperature profiles in soil as functions of time (b) The temperature profiles zoomed-in to show the pulse at the surface reaching 5m on the 73rd day.
Fig. 8. Mass balance errors. (a) Cumulative relative errors as given by equation (15a) (b) Instantaneous error during each time step Δt (c) Moisture flux incident on the upper boundary during each time step.
Fig. 9. Energy balance errors. (a) Cumulative relative errors as given by equation (15b) (b) Instantaneous error during each time step Δt (c) Energy flux incident on the upper boundary during each time step.
Fig.10. Propagation of moisture and heat: (a) Temperature profiles and (b) Moisture profiles during the 43-day model run. (c) Soil water retention curve from the two-parameter junction model of Rossi and Nimmo (Rossi and Nimmo, 1994) at soil temperature 295 K.
Fig. 11. Comparison of analytic and numerical solution. (a) Volumetric soil moisture profiles. (b) Temperature profiles in soil as functions of time.

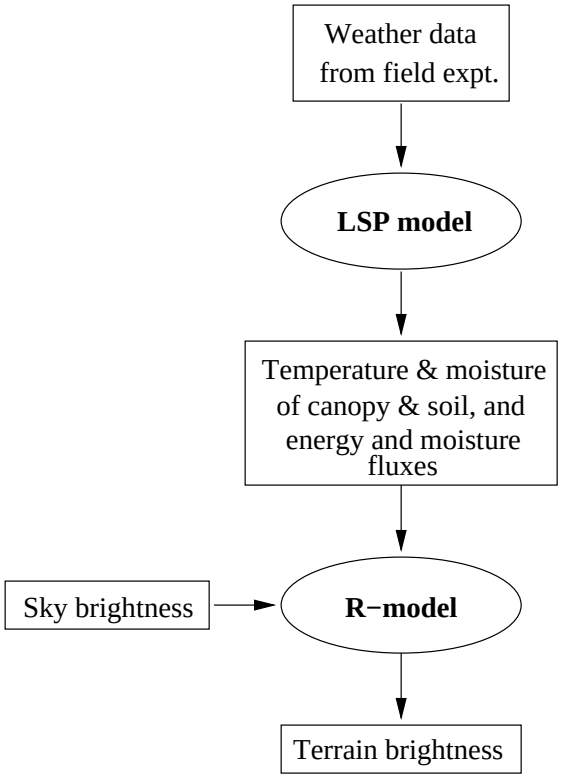
Weather data
from field expt.
LSP model
Temperature & moisture
of canopy & soil, and
energy and moisture
fluxes
Sky brightness
R−model
Terrain brightness

Fig. 1.

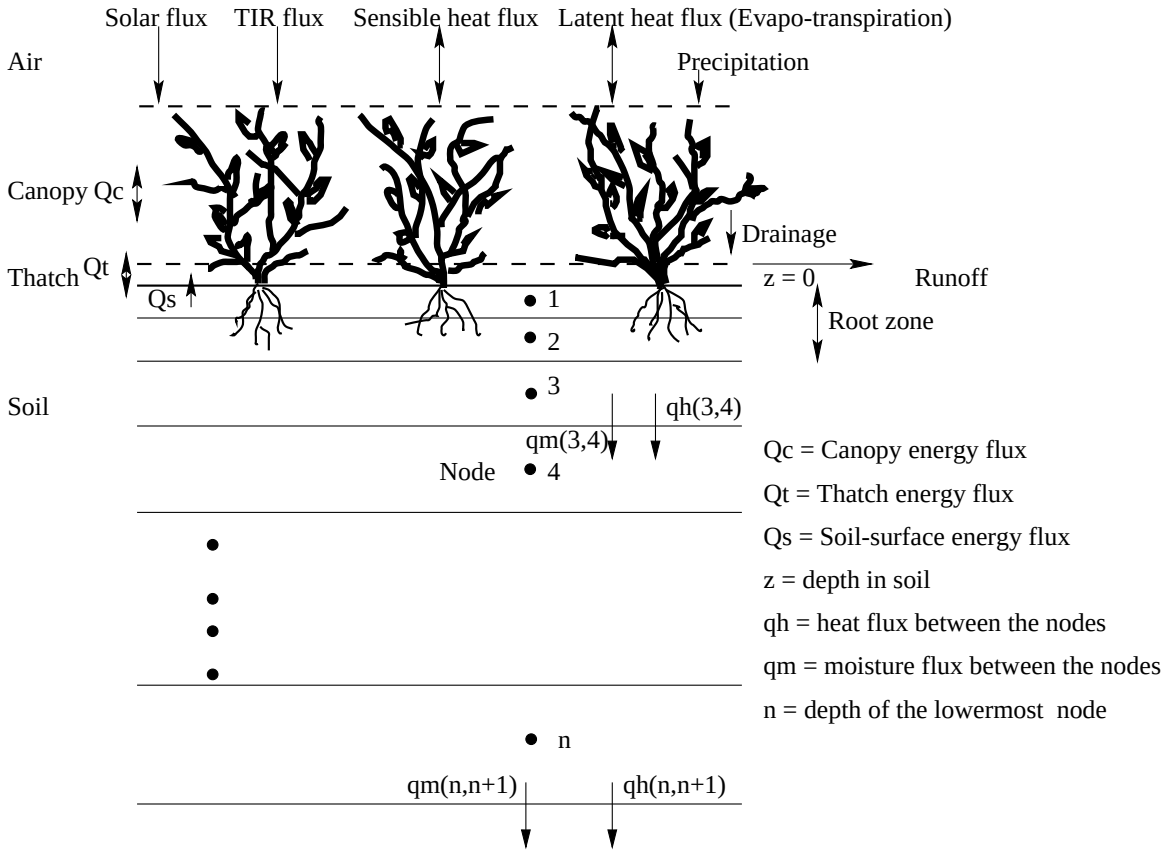
Solar flux
TIR flux
Sensible heat flux
Latent heat flux (Evapo-transpiration)
Air
Precipitation
Canopy Qc
Drainage
Thatch Qt
z = 0
Runoff
Qs
1
Root zone
2
3
Soil
qh(3,4)
qm(3,4)
Node
4
Qc = Canopy energy flux
Qt = Thatch energy flux
Qs = Soil-surface energy flux
z = depth in soil
qh = heat flux between the nodes
qm = moisture flux between the nodes
n = depth of the lowermost node
n
qm(n,n+1)
qh(n,n+1)

Fig. 2.

For every soil block, j, and time increment, ∂t,

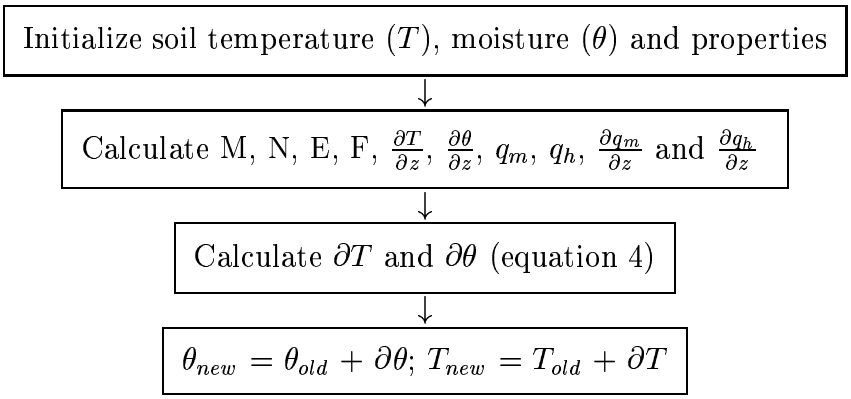

where, $\frac{\partial T}{\partial z}(j) = \frac{T(j+1)-T(j)}{z(j+1)-z(j)}$, $\frac{\partial \theta}{\partial z}(j) = \frac{\theta(j+1)-\theta(j)}{z(j+1)-z(j)}$
$\frac{\partial q_h}{\partial z}(j) = \frac{q_h(j,j+1)-q_h(j-1,j)}{z(j+1)-z(j)}$, $\frac{\partial q_m}{\partial z}(j) = \frac{q_m(j,j+1)-q_m(j-1,j)}{z(j+1)-z(j)}$

Fig. 3.

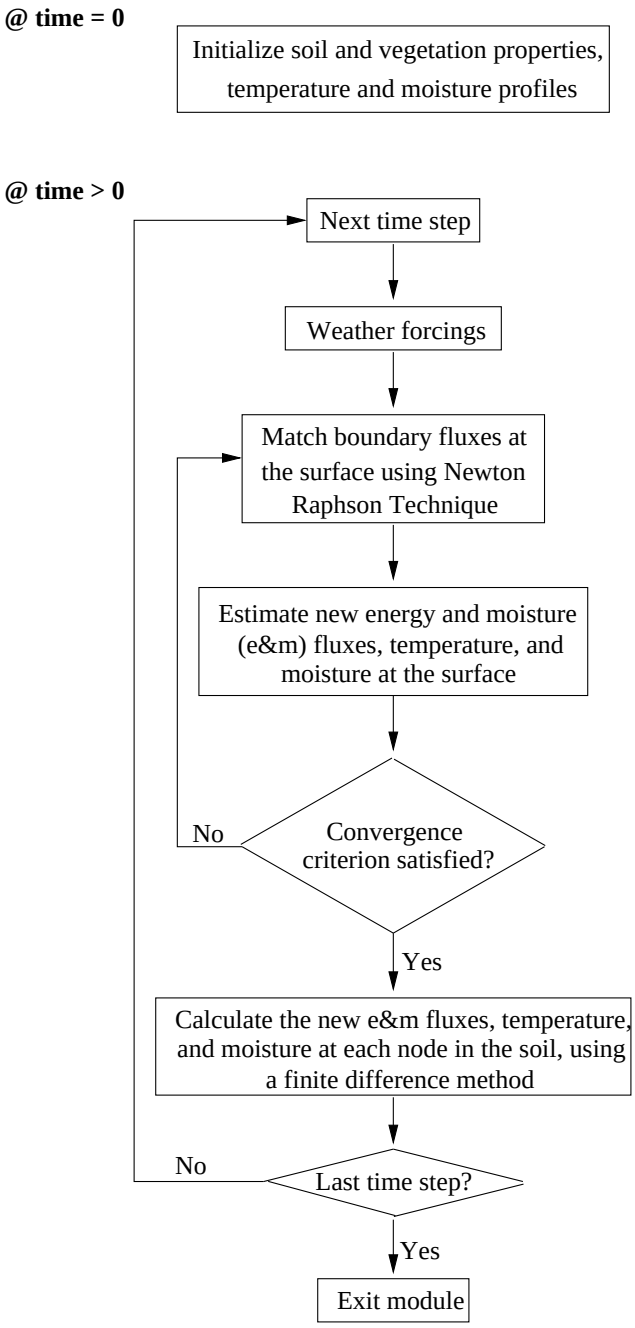
@ time = 0
Initialize soil and vegetation properties, temperature and moisture profiles
@ time > 0
Next time step
Weather forcings
Match boundary fluxes at the surface using Newton Raphson Technique
Estimate new energy and moisture (e&m) fluxes, temperature, and moisture at the surface
Convergence criterion satisfied?
No
Yes
Calculate the new e&m fluxes, temperature, and moisture at each node in the soil, using a finite difference method
Last time step?
No
Yes
Exit module

Fig. 4.

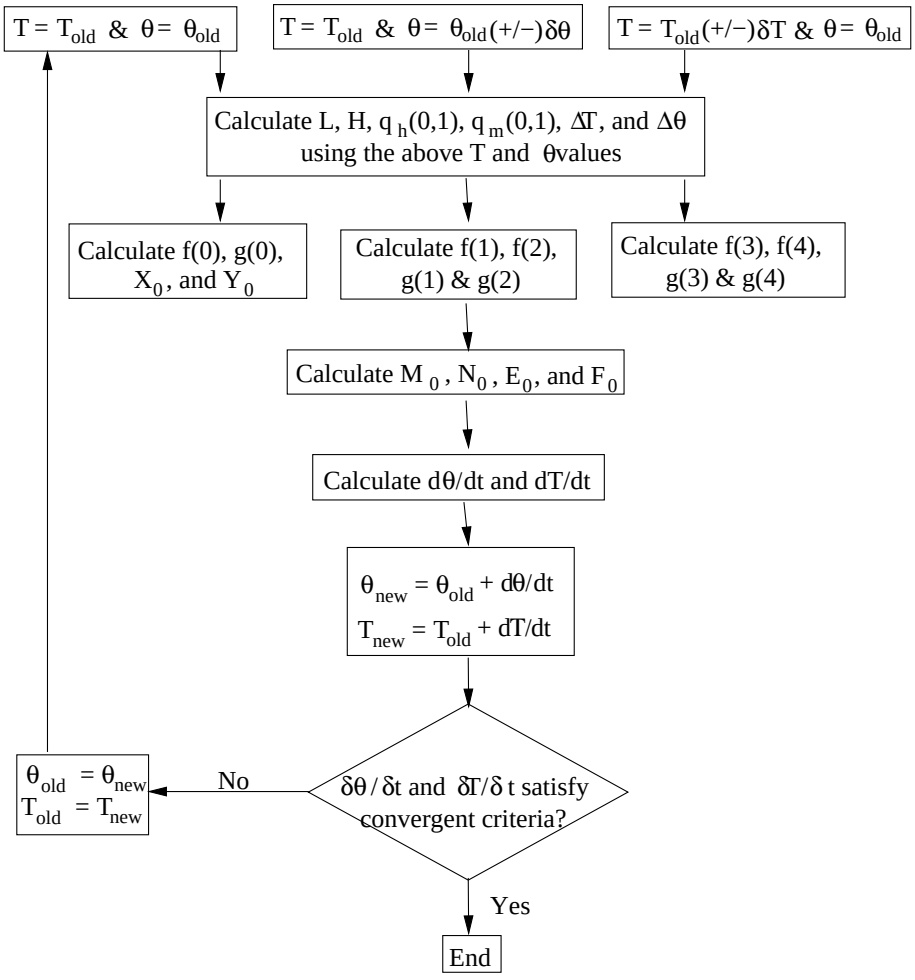

where, $f = M_1\Delta\theta + E_1\Delta T$ $\quad g = N_1\Delta\theta + F_1\Delta T$

$M_0 = \frac{f(2)-f(1)}{2\delta\theta}$ $\quad E_0 = \frac{f(4)-f(3)}{2\delta\theta}$

$N_0 = \frac{g(2)-g(1)}{2\delta T}$ $\quad F_0 = \frac{g(4)-g(3)}{2\delta T}$

$\Delta\theta = \theta - \theta_1$ $\quad \delta\theta = 1\text{x}10^{-10}$

$\Delta T = T - T_1$ $\quad \delta T = 1\text{x}10^{-10}$

L = Latent heat flux $\quad$ H = Sensible heat flux

• Subscripts 0 and 1 refer to the parameter values for the current and the previous time steps, respectively.

Fig. 5.

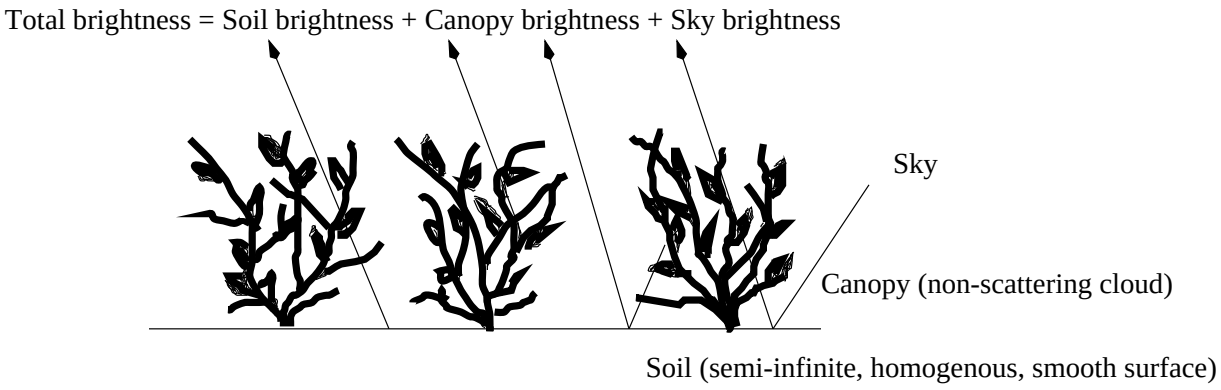
Total brightness = Soil brightness + Canopy brightness + Sky brightness
Sky
Canopy (non-scattering cloud)
Soil (semi-infinite, homogenous, smooth surface)

Fig. 6.

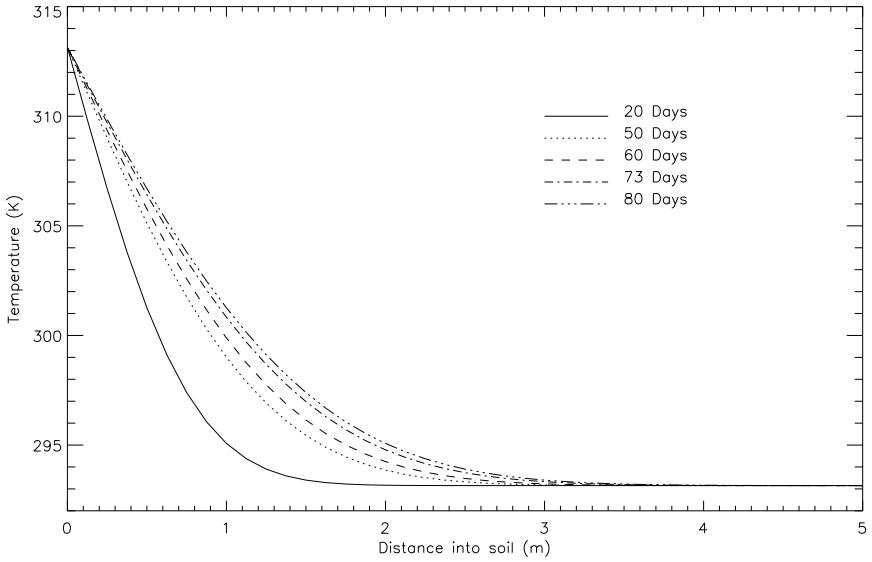
315
310
305
300
295
Temperature (K)
0
1
2
3
4
5
Distance into soil (m)
20 Days
50 Days
60 Days
73 Days
80 Days

(a)

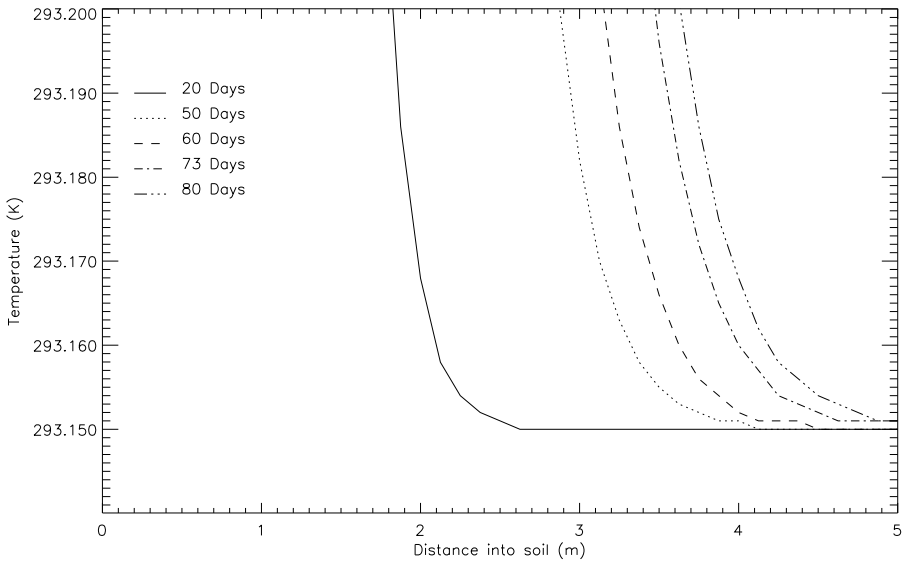
293.200
293.190
293.180
293.170
293.160
293.150
Temperature (K)
0
1
2
3
4
5
Distance into soil (m)
20 Days
50 Days
60 Days
73 Days
80 Days

(b)

Fig. 7.

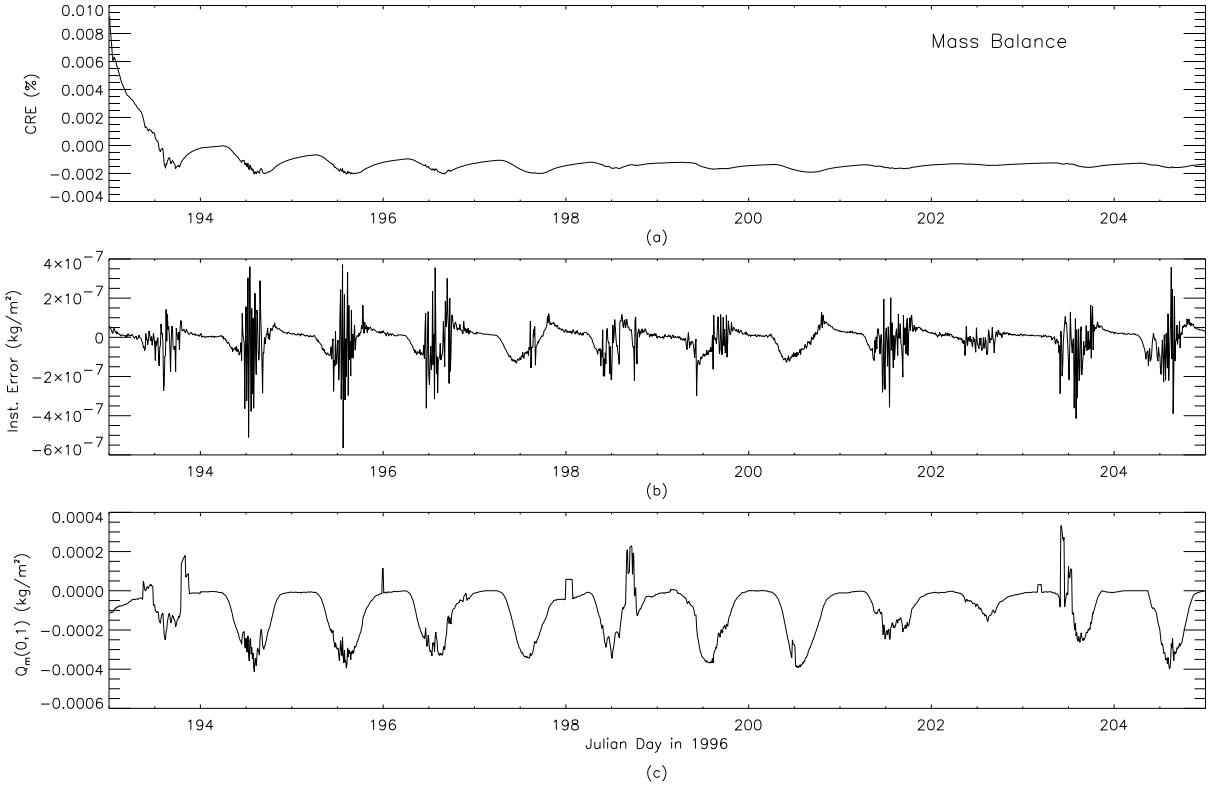
Mass Balance
CRE (%)
0.010
0.008
0.006
0.004
0.002
0.000
−0.002
−0.004
194
196
198
200
202
204
(a)
Inst. Error (kg/m²)
4×10⁻⁷
2×10⁻⁷
0
−2×10⁻⁷
−4×10⁻⁷
−6×10⁻⁷
194
196
198
200
202
204
(b)
Q_m(0,1) (kg/m²)
0.0004
0.0002
0.0000
−0.0002
−0.0004
−0.0006
194
196
198
200
202
204
Julian Day in 1996
(c)

Fig. 8.

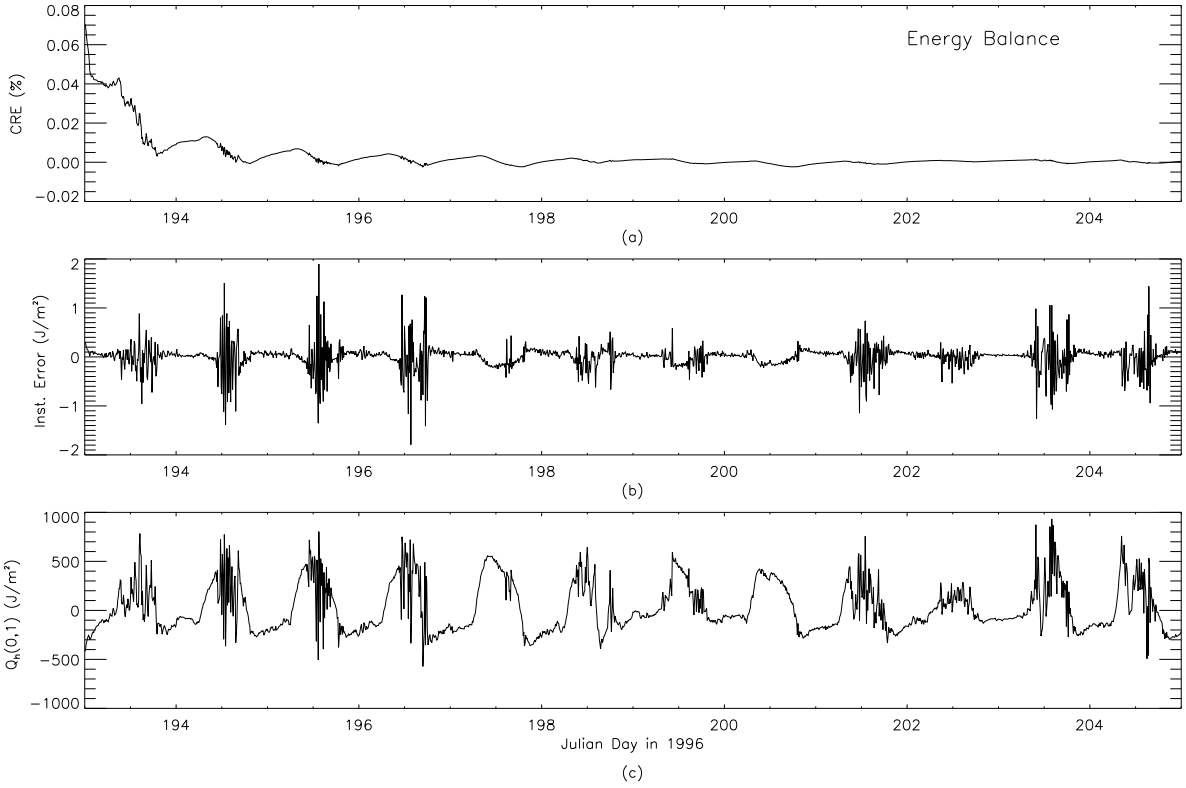
Energy Balance
CRE (%)
0.08
0.06
0.04
0.02
0.00
−0.02
194
196
198
200
202
204
(a)
Inst. Error (J/m²)
2
1
0
−1
−2
194
196
198
200
202
204
(b)
Q_h(0,1) (J/m²)
1000
500
0
−500
−1000
194
196
198
200
202
204
Julian Day in 1996
(c)

Fig. 9.

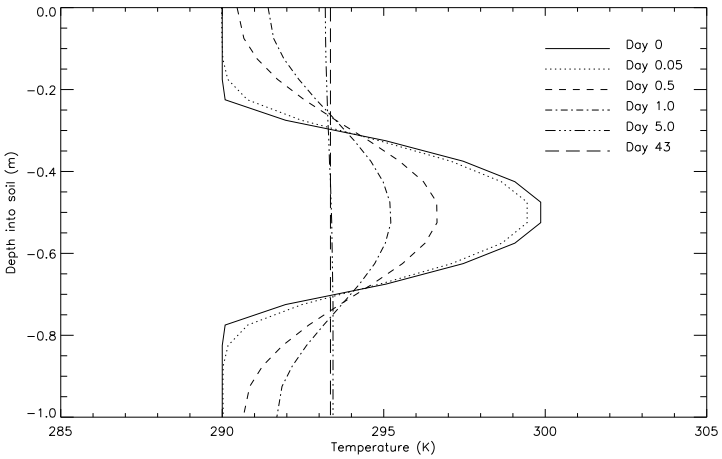
Day 0
Day 0.05
Day 0.5
Day 1.0
Day 5.0
Day 43
Depth into soil (m)
Temperature (K)
0.0
−0.2
−0.4
−0.6
−0.8
−1.0
285
290
295
300
305

(a)

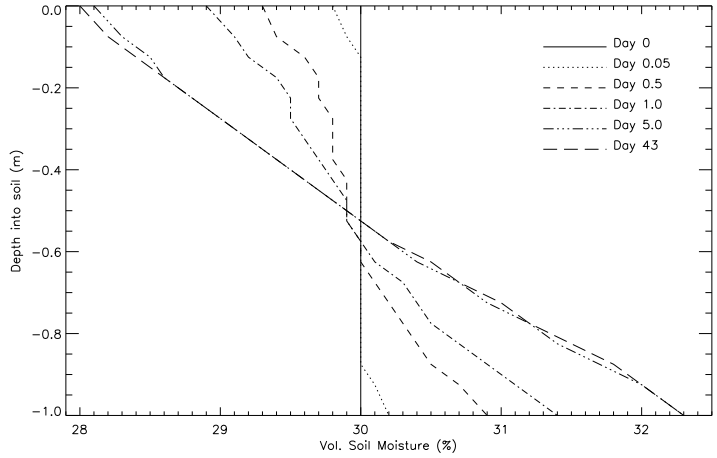
Day 0
Day 0.05
Day 0.5
Day 1.0
Day 5.0
Day 43
Depth into soil (m)
Vol. Soil Moisture (%)
0.0
−0.2
−0.4
−0.6
−0.8
−1.0
28
29
30
31
32

(b)

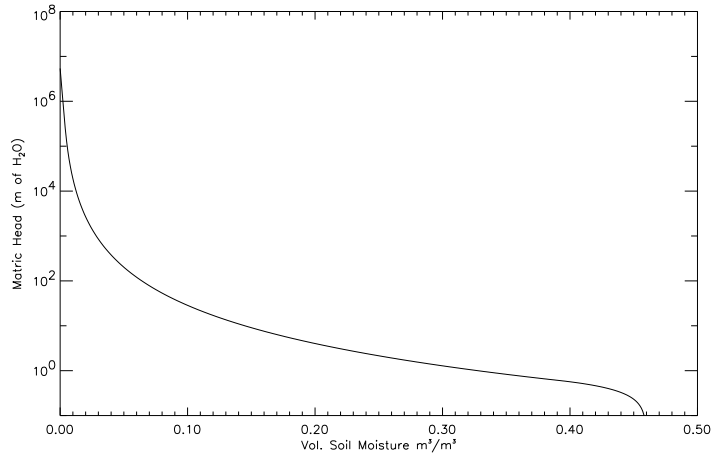
Matric Head (m of H2O)
Vol. Soil Moisture m³/m³
10^8
10^6
10^4
10^2
10^0
0.00
0.10
0.20
0.30
0.40
0.50

(c)

Fig. 10.

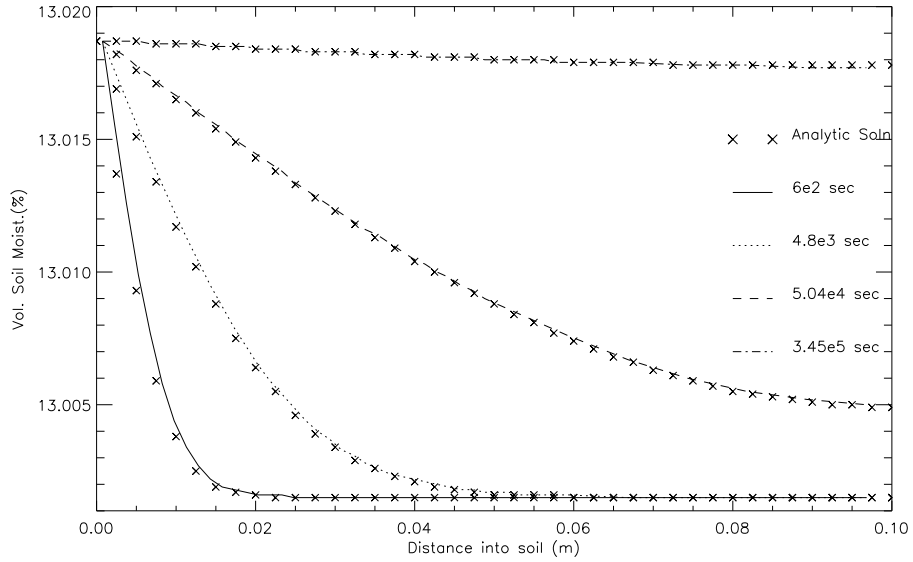
13.020
13.015
13.010
13.005
Vol. Soil Moist.(%)
0.00
0.02
0.04
0.06
0.08
0.10
Distance into soil (m)
Analytic Soln
6e2 sec
4.8e3 sec
5.04e4 sec
3.45e5 sec

(a)

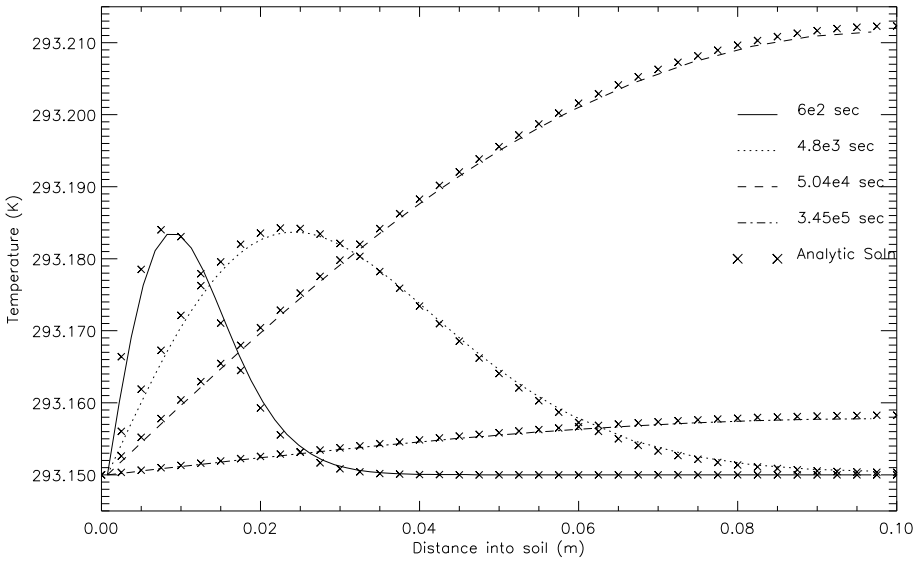
293.210
293.200
293.190
293.180
293.170
293.160
293.150
Temperature (K)
0.00
0.02
0.04
0.06
0.08
0.10
Distance into soil (m)
6e2 sec
4.8e3 sec
5.04e4 sec
3.45e5 sec
Analytic Soln

(b)

Fig. 11.

Properties	**Values**
Texture	3.9% sand, 65.1% silt, 31.0% clay
Porosity	0.46
Sat. Hydr. Cond.	4.74x10^{-7} m/sec
Field Capacity	0.294 % by volume

Table 1
Soil constitutive properties used for model simulation to evaluate errors in mass and energy balance.

Properties/Parameters	**Values**
Porosity	0.495
Thermal Cond.	0.165 $J/m.K.sec$
Thermal Cap.	1.673663x10^6 $J/m^3.K$
Latent heat of vap.(L)	2.45616x10^6 J/kg
σ_c	0.274 m^3/kg
ω_c	0 K^{-1}
D	3.63x10^{-8} m^2/sec
$\mathbb{D}$	9.89x10^{-8} m^2/sec
λ_c	0 $kg/m^3.K$
ν_c	395.286 $K.m^3/kg$

Table 2
Soil properties for Yolo light clay and other parameters used to calculate the analytic solution. The same soil properties were also used by the numerical model.